Cardiac myosin missense mutations cause dilated cardiomyopathy in mouse models and depress molecular motor function

Joachim P. Schmitt*†, Edward P. Debold‡, Ferhaan Ahmad*§, Amy Armstrong‡, Andrea Frederico‡, David A. Conner*, Ulrike Mende¶‖, Martin J. Lohse†, David Warshaw‡, Christine E. Seidman*¶**††, and J. G. Seidman*

*Department of Genetics and Howard Hughes Medical Institute, Harvard Medical School, Boston, MA 02115; ‡Department of Molecular Physiology and Biophysics, University of Vermont, Burlington, VT 05405; †Institute of Pharmacology and Toxicology, University of Würzburg, 97087 Würzburg, Germany; and ¶Cardiovascular Division and **Howard Hughes Medical Institute, Brigham and Women's Hospital, Boston, MA 02115

Contributed by Christine E. Seidman, July 28, 2006

Dilated cardiomyopathy (DCM) leads to heart failure, a leading cause of death in industrialized nations. Approximately 30% of DCM cases are genetic in origin, with some resulting from point mutations in cardiac myosin, the molecular motor of the heart. The effects of these mutations on myosin's molecular mechanics have not been determined. We have engineered two murine models characterizing the physiological, cellular, and molecular effects of DCM-causing missense mutations (S532P and F764L) in the α-cardiac myosin heavy chain and compared them with WT mice. Mutant mice developed morphological and functional characteristics of DCM consistent with the human phenotypes. Contractile function of isolated myocytes was depressed and preceded left ventricular dilation and reduced fractional shortening. In an *in vitro* motility assay, both mutant cardiac myosins exhibited a reduced ability to translocate actin (V_{actin}) but had similar force-generating capacities. Actin-activated ATPase activities were also reduced. Single-molecule laser trap experiments revealed that the lower V_{actin} in the S532P mutant was due to a reduced ability of the motor to generate a step displacement and an alteration of the kinetics of its chemomechanical cycle. These results suggest that the depressed molecular function in cardiac myosin may initiate the events that cause the heart to remodel and become pathologically dilated.

animal models | biophysics | genetics | single molecule | laser trap

Dilated cardiomyopathy (DCM) is an early step in the pathway leading to heart failure, the leading cause of human morbidity and mortality (1, 2). Although etiological factors such as ischemia and diabetes can result in DCM, at least 30% of cases are genetic in origin, with mutations found in sarcomeric proteins associated with the cytoskeletal and contractile systems (3). Clinically, DCM is characterized by myocardial hypertrophy, thin-walled ventricles, and myocyte hypoplasia (2, 4). Dilated hearts are hypocontractile, with systolic dysfunction leading to a reduced ejection fraction: a hallmark of a failing heart (2, 3). Only recently have autosomal dominant missense mutations to the β-cardiac myosin heavy chain (MHC) been identified that result in DCM (5, 6). Because the primary defect resides within the heart's molecular motor, we hypothesized that altered cardiac contractile function in DCM hearts might reflect changes in the mutant myosin's ability to generate force and motion as it cyclically interacts with actin during its hydrolysis of ATP.

To investigate the impact of two distinct DCM-causing MHC mutations (S532P and F764L) on cardiac myosin's molecular performance, we have genetically engineered these missense mutations separately into the murine α-cardiac MHC gene, the human β-MHC homolog, to generate two separate DCM knockin mouse models. In addition to cardiac dilation and dysfunction, defects in isolated myocyte contractility were observed that are consistent with DCM. Interestingly, defects at the whole-heart and cellular levels were correlated with reduced mutant cardiac myosin ATPase activity and actin filament velocity as determined in an *in vitro* motility assay, a model system for unloaded myocardial shortening (7). The lower actin filament velocity was attributed to alterations in both the inherent motion generation and kinetics of a single myosin molecule's interactions with actin in the laser trap assay.

Results and Discussion

Mouse Models, Cardiac Morphology, and Function. Two DCM mutations, one in the actin-binding domain (S532P; Fig. 1*A*) and another in the converter (F764L; Fig. 1*A*) (8), were engineered separately into the murine α-cardiac MHC gene by homologous recombination in ES cells (Fig. 5, which is published as supporting information on the PNAS web site). Heterozygous (designated $MHC^{F764L/+}$ and $MHC^{S532P/+}$) and homozygous (designated $MHC^{F764L/F764L}$ and $MHC^{S532P/S532P}$) offspring are fully viable and fertile, and they survive >1 year, albeit with indications of DCM (Fig. 1*B*, Table 1, and data not shown).

To characterize their cardiac phenotype, DCM mutant mice were evaluated by serial echocardiograms (Table 1). As in humans who are heterozygous for these myosin mutations, heterozygous mutant mice demonstrate gradual increases in left ventricle (LV) chamber size. These increases were initially observed in some mutant mice by age 12 weeks and in all mutant animals by 50 weeks of age (Table 1 and data not shown). Despite changes in cardiac morphology, there were negligible changes in fractional shortening or cardiac function (Table 1). The onset of disease was more pronounced in $MHC^{F764L/+}$ mice than in $MHC^{S532P/+}$ mice. These findings are consistent with the clinical features of most patients with the S532P mutation, who show slow disease progression and live into their 70s; patients carrying the F764L mutation display evidence of disease during childhood, which progresses slowly during adulthood (6).

Homozygous mutant mice progressed rapidly to DCM and developed more contractile dysfunction at much younger ages (≈12 weeks) than heterozygous mice (Table 1). Both $MHC^{F764L/F764L}$ and $MHC^{S532P/S532P}$ homozygous mice developed significant cardiac

Author contributions: J.P.S. and E.P.D. contributed equally to this work; D.W., C.E.S., and J.G.S. designed research; J.P.S., E.P.D., F.A., A.A., A.F., D.A.C., U.M., M.J.L., and C.E.S. performed research; J.P.S., E.P.D., F.A., D.W., C.E.S., and J.G.S. analyzed data; and J.P.S., E.P.D., D.W., C.E.S., and J.G.S. wrote the paper.

The authors declare no conflict of interest.

Abbreviations: MHC, myosin heavy chain; DCM, dilated cardiomyopathy; HCM, hypertrophic cardiomyopathy; LV, left ventricle.

§Present address: Cardiovascular Institute, University of Pittsburgh, Pittsburgh, PA 15213.

‖Present address: Rhode Island Hospital and Brown Medical School Cardiovascular Research Center, Providence, RI 02903.

††To whom correspondence should be addressed at: Department of Genetics, Harvard Medical School, 77 Avenue Louis Pasteur, Boston, MA 02115. E-mail: cseidman@genetics.med.harvard.edu.

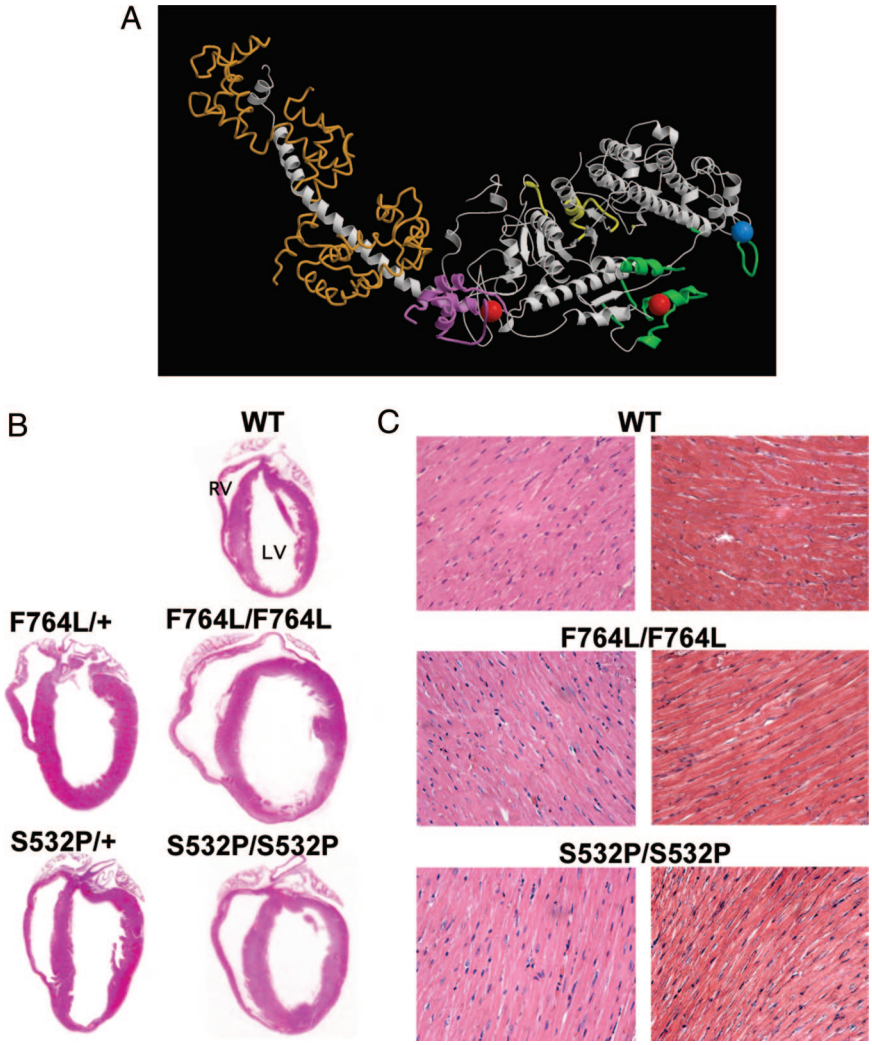

Fig. 1. Location of the S532P and F764L missense mutations in cardiac MHC and the structure of hearts expressing these mutant proteins. (*A*) Three-dimensional structure of the S1 domain of chicken MHC with associated myosin light chains (gold) indicating residues that interact with ATP (yellow), and the locations of the DCM mutations S532P (red circle) in the actin-binding domain (green) and F764L (red circle) in the converter region (magenta), as well as the R403Q HCM mutation (blue circle) in a loop within the actin-binding domain. (*B*) Longitudinal sections from 30- to 40-week-old WT, heterozygous (S532P/+; F764L/+), and homozygous (S532P/S532P; F764L/F764) mutant hearts. Note the enlarged ventricles but normal atrial size in mutant hearts. (*C*) Cardiac histology was assessed in 20- to 30-week-old WT and homozygous (S532P/S532P; F764L/F764) mutant hearts by hematoxylin/eosin (*Left*) and Masson trichrome (*Right*) staining.

dilation, [i.e., increased LV chamber size, reduced fractional shortening, and contractile dysfunction (Table 1)]. Histological analyses of heterozygous and homozygous cardiac tissue, although consistent with the diagnosis of DCM and elongated myocytes, demonstrated no myofibrillar disarray or fibrosis in young mice (Fig. 1 and Table 2) or in 50-week-old mice (data not shown), as observed previously in models of hypertrophic cardiomyopathy (HCM) (9, 10) or in other forms of DCM (11).

Isolated cardiac myocytes from 8-week-old heterozygous DCM mice have impaired contractile function, as evidenced by a reduced extent and rate of shortening compared with WT mice (Table 2). Although the rate of relaxation was normal in $MHC^{S532P/+}$ myocytes, it was significantly slower in $MHC^{F764L/+}$ myocytes. These perturbations to cellular contractile performance were observed in advance of any cardiac dilation (Table 2). Thus, the primary insult to the myosin motor diminishes cellular contractile capacity and is reflected in impaired cardiac performance (Tables 1 and 2).

Cardiac Myosin Molecular Performance. Isolated cardiac myosin was used to determine whether the DCM-causing mutations affected myosin's ATP hydrolysis and molecular mechanics. The maximum actin-activated ATPase activity for the F764L mutant myosin was significantly reduced compared with WT, although it was not significant for the S532P mutant (Fig. 2). There was no apparent effect on either the basal ATPase activity or K_m for either mutant (Table 3). However, our ability to detect an effect on K_m was likely limited by the actin concentrations used in the ATPase assay (Fig. 2). All *in vitro* myosin studies were performed with mutant cardiac myosin isolated from homozygous mutant animals, which have no WT α-cardiac MHC, thus reducing contamination by WT protein. In addition, we characterized the motion- and force-generating capacity of the mutant myosin in an *in vitro* motility assay in which the movement of individual fluorescently labeled actin filaments over a surface coated with individual myosin molecules was assessed (12, 13). The velocity of actin movement (V_{actin}) was significantly reduced for the mutant myosins, with F764L myosin 20% lower than WT and S532P myosin 40% lower than WT, suggesting that the slower rates of myocyte shortening are due, at least in part, to altered molecular motor function (Table 3).

Alterations to actin filament motion must reflect the impact

Table 1. Cardiac morphology and function of WT, heterozygous MHC$^{S532P/+}$ and MHC$^{F764L/+}$, and homozygous MHC$^{S532P/S532P}$ and MHC$^{F764L/F764L}$ mice assessed by echocardiography

Characteristic	WT	S532P/+	*P*	F764L/+	*P*	WT	S532P/S532P	*P*	F764L/F764L	*P*
No. of mice	9	8	—	6	—	49	7	—	12	—
Age, weeks	48 ± 16	48 ± 4	—	48 ± 1	—	10–30	10–30	—	10–30	—
LVWT, mm	0.92 ± 0.10	1.0 ± 0.04	0.04	0.95 ± 0.10	NS	0.90 ± 0.09	0.90 ± 0.16	NS	1.00 ± 0.15	0.002
LVEDD, mm	2.61 ± 0.24	3.00 ± 0.74	0.08	3.25 ± 0.55	0.003	2.62 ± 0.42	3.61 ± 0.49	<0.0001	3.21 ± 0.34	<0.0001
LVESD, mm	0.72 ± 0.34	0.94 ± 0.76	NS	1.19 ± 0.57	0.03	0.78 ± 0.29	1.90 ± 0.31	<0.0001	1.47 ± 0.31	<0.0001
FS, %	73 ± 11	71 ± 14	NS	65 ± 12	0.079	73 ± 11	47 ± 4	<0.0001	54 ± 7	<0.0001

Values are means ± SD. LVWT, LV wall thickness at end diastole; LVEDD, LV end diastolic diameter; LVESD, LV end systolic diameter; FS, fractional shortening; NS, not significant; —, not applicable.

of the mutation on the molecular mechanics of the myosin motor. Specifically, V_{actin} is related to the displacement generated by the myosin powerstroke (i.e., the step size, d) and the duration that myosin remains attached to actin after the step (t_{on}), so that V_{actin} is proportional to d/t_{on} (14). We measured both d and t_{on} at the level of a single myosin molecule by using the laser trap assay (Fig. 3). For the S532P mutant, more than half of the 40% reduction in V_{actin} can be accounted for by the 24% smaller step size (Table 3). The remaining decrease in V_{actin} may be explained by the 24% longer duration of attachment observed in the laser trap (Table 3). However, in the laser trap, where 10 μM MgATP is used to enhance detection of individual events, t_{on} is determined by both the rate of MgADP release and subsequent binding of MgATP (14, 15), whereas V_{actin} at saturating [MgATP] is limited only by the rate of ADP release (14). Therefore, the individual kinetic step(s) affected by the mutation cannot be delineated. Despite this information, a single point mutation in the actin-binding domain did affect the motor's inherent motion generation, d, and one or more transition rates between states in the actomyosin ATPase cycle that are determinants of t_{on}.

The myosin step size is due to a rotation of the myosin light chain binding domain or neck that acts as a rigid lever to amplify motions originating within myosin's ATP-binding site (16). With the S532P mutation existing in the actin-binding domain, some distance from the myosin neck, the change in step size was surprising, whereas an effect on the duration of the actin–myosin interaction might have been predicted. It is possible that the S532P mutation may have disrupted normal actomyosin contacts, weakening myosin's attachment to actin so that full cleft closure within the head is prevented, a process that may be required for full rotation of the lever arm (17). Although the F764L mutant exhibited a 20% reduction in V_{actin} (Table 3), the single-molecule measurements could not detect any changes in either d or t_{on}. If, as for the S532P mutant myosin, both mechanical and kinetic components contribute equally to the 20% reduction in V_{actin}, then 10% changes in both d and t_{on} are below our detection limits (18). Regardless of the molecular mechanism, both the S532P and the F764L mutations share a common phenotype by having reduced actin filament velocities and actomyosin ATPase activities (Fig. 2 and Table 3).

In addition to the mutations' effect on V_{actin}, we investigated whether the mutant myosin's force-generating capacity was altered. We estimated myosin's average maximum isometric force (F_{avg}) by using an *in vitro* motility mixtures assay (19): a molecular tug of war in which fluorescently labeled actin filaments are observed moving over a surface coated with a myosin mixture composed of mutant or WT cardiac myosin and the slower smooth-muscle myosin. We chose smooth-muscle myosin because of its known high force-generating capacity compared with other muscle myosins (19, 20). In this assay, V_{actin} is a result of the two different myosins interacting simultaneously with the same actin filament and is related to differences in the relative force-generating capacities for the two myosins. Differences in F_{avg} determine the curvature of the relationship between V_{actin} and the myosin mixture ratio (Fig. 4 and ref. 19). The V_{actin}:myosin mixture curve for the cardiac WT/smooth-muscle myosin mixture is concave downward (see Fig. 4). Analysis of these data suggests that mouse α-cardiac myosin generates half the F_{avg} of smooth-muscle myosin, as previously reported (19–21). In addition, with the curvature for all of the V_{actin}:myosin mixtures being similar for all cardiac myosins tested (see Fig. 4), it appears that F_{avg} is the same for F764L, S532P, and WT myosins (Table 3).

For the heart to function as a pump, it must generate sufficient power for blood to perfuse through the vascular system. Power is the product of force and velocity. By using V_{actin} and F_{avg} for the mutant myosins, the estimated power-generating capacity is apparently diminished by as much as 20% for the F764L and by as much as 40% for the S532P mutants relative to WT. However, peak power typically occurs at ≈30% of maximal isometric force in muscle (22); therefore, a true determination of whether power is altered in these mutant myosins will require characterization of the entire force:velocity relationship (23).

In addition to the mutations characterized here that lead to DCM, >100 missense mutations in the β-cardiac MHC have been identified that result in HCM (24). In contrast to DCM hearts, HCM hearts are characterized by thick ventricular walls that exhibit enhanced contractile function and impaired relax-

Table 2. Myocyte characteristics from 8-week-old WT, MHC$^{S532P/+}$, and MHC$^{F764L/+}$ mice

Characteristic	WT	S532P/+	*P*	F764L/+	*P*
No. of cells	70	51	—	58	—
Cell length, μm	112 ± 21	113 ± 22	NS	121 ± 26	0.02
dL/dt contraction, μm·s^{-1}	114 ± 63	90 ± 61	0.04	79 ± 48	0.001
Cell shortening, %	5.05 ± 3.13	3.86 ± 2.57	0.03	2.72 ± 1.67	<0.0001
dL/dt relaxation, μm·s^{-1}	67 ± 58	60 ± 73	NS	44 ± 42	0.02
T_{50} baseline, ms	171 ± 49	177 ± 74	NS	155 ± 65	NS

Values are mean ± SD. dL/dt contraction, velocity of cell shortening; dL/dt relaxation, velocity of cell relengthening; T_{50} baseline, time to 50% maximum relaxation; NS, not significant; —, not applicable.

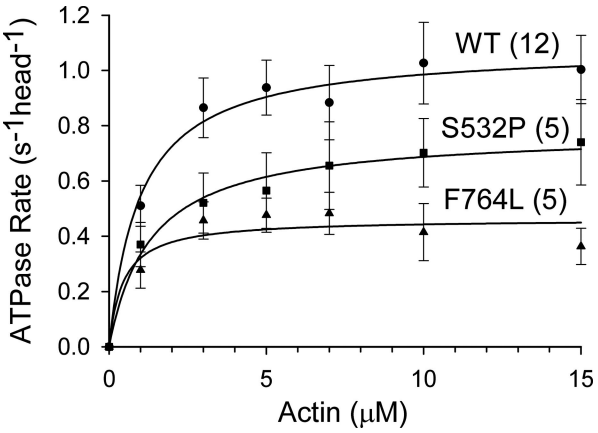

Fig. 2. Actin-activated ATPase activity versus actin concentration for WT and the mutant myosins S532P and F764L. The data at each actin concentration is the mean ± SE of data from the number of hearts displayed in parenthesis next to the label. These curves are the fit to the Michaelis–Menten relationship with the mean values for V_{max} and K_m presented in Table 3.

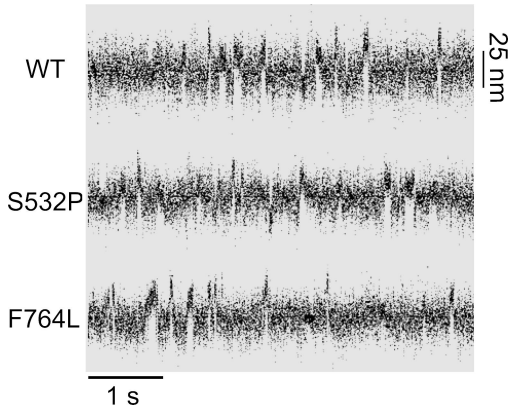

Fig. 3. Representative unitary bead displacement records obtained from optical trapping experiments for WT and the mutant myosins S532P and F764L. The traces demonstrate bead movement as detected by the quadrant photodiode detector in the three-bead laser trap assay (see *Materials and Methods*). Myosin binding events are marked by rapid deflections in the displacement trace and a reduction in Brownian motion caused by the added stiffness of the myosin molecule to the bead–actin–bead assembly. Nineteen to 39 independent traces (≈2 min in duration) were obtained for each myosin type. Estimates of the step size and duration of strong binding were derived by using the mean-variance technique (18) and are reported in Table 3.

ation (25, 26). Do the various myosin mutations differentially impact myosin performance to account for such dramatically different clinical phenotypes associated with DCM and HCM? HCM-causing mutations, especially the R403Q mutant, enhance rather than compromise function (10, 15, 19, 28, 29). Direct comparison of the mutant myosins described here with data obtained by our laboratories from mutant R403Q myosin isolated from a mouse model using all of the identical assays (29) demonstrates that V_{actin}, F_{avg}, and actomyosin ATPase activity all are enhanced for R403Q myosin compared with controls. The enhanced function was also seen in myosin obtained from human β-cardiac samples (15, 27), suggesting that the mutation has its effects regardless of the myosin backbone.

Conclusions. The primary insult to the cardiac myosin motor as a result of the S532P or F764L mutations leads to DCM in the mouse model, faithfully reproducing the human phenotype. The compromised enzymatic and mechanical activities at the molecular motor level are the most likely determinants of alterations in the mechanical performance at the myocyte and whole-heart levels. How any mutant-dependent changes in specific mechanical and/or enzymatic properties are linked to the dramatic myocardial remodeling is far from certain. However, there must exist numerous parallel signaling pathways within the myocyte that are sensitive to myocyte mechanics, as well as its energy (i.e., ATP) consumption (30–32), so that alterations to these mechanical and/or enzymatic indices must serve as the trigger to begin the remodeling process.

That missense mutations in the cardiac MHC gene resulting in a differential primary insult to the performance of the heart's molecular motor is remarkable. Although comprised mechanical function is not a common theme for either DCM or HCM, based on the present data and our prior work, we conclude that DCM mutants have diminished molecular motor function, whereas HCM mutants may have enhanced molecular motor function. This differential effect is not limited to myosin mutations but appears also in mutations within the actin-regulatory system (33), so that more generally altered sarcomeric function dictates phenotypic outcome. Differential changes in the molecular motor performance may be predictive of the clinical outcome to cardiac function and pathology. In addition, these studies offer the potential for developing treatments that may overcome the inherent program to remodel the heart by increasing, or in some cases reducing, the contractile machinery's ability to generate power.

Table 3. Ensemble and single-molecule mechanical properties

Property	WT	S532P	*P*	F764L	*P*
V_{actin}, μm·s^{-1}	4.2 ± 0.7 (20)	2.4 ± 0.3 (18)*	0.0001	3.4 ± 0.4 (6)*	0.01
Basal ATPase V_{max}, s^{-1}·head^{-1}	0.02 ± 0.01 (12)	0.05 ± 0.3 (5)	NS	0.02 ± 0.01 (5)	NS
K_m, μM	1.2 ± 1.0 (12)	2.2 ± 2.0 (5)	NS	1.1 ± 0.6 (5)	NS
d, nm	7.6 ± 2.2 (28)	5.8 ± 2.4 (39)*	0.005	7.0 ± 2.0 (19)	NS
t_{on}, ms	29 ± 6 (26)	36 ± 11 (39)*	0.003	29 ± 7 (19)	NS
F_{avg}, normalized	1.0 ± 0.1 (2)	0.8 ± 0.1 (2)	NS	0.8 ± 0.1 (2)	NS

See *Materials and Methods* for detailed procedures for determination of all parameters. Actin filament velocities (V_{actin}) are means ± SD from the number of mouse hearts (shown in parentheses). Basal ATPase, ATPase activity in the absence of actin; V_{max} ATPase, maximum actin-activated value and K_m determined by Michaelis–Menten fit to the ATPase versus actin concentration (see Fig. 2) with the number of hearts in parentheses; *d*, myosin step size; t_{on}, duration of myosin attachment to actin after the powerstroke, presented as mean ± SD with the number of myosin molecules shown in parentheses. Values of F_{avg} are means ± SE of the estimate as determined from the fit to the mixtures assay data (see Fig. 4).

*Differences were quantified by using a one-way ANOVA with a Student–Neuman–Keuls post hoc test used to locate significant differences at $P < 0.05$.

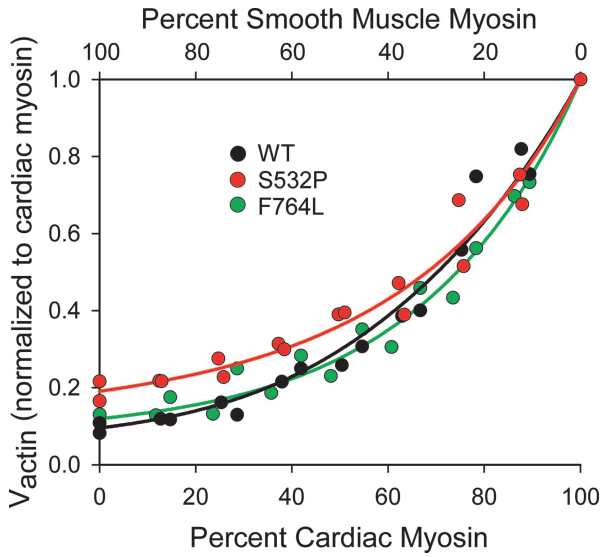

Fig. 4. *In vitro* motility mixture assay for estimating the relative average force (F_{avg}) for the WT and mutant S532P and F764L cardiac myosins compared with smooth-muscle myosin. The relationships between V_{actin} and the percentage of fast (cardiac) and slow (smooth muscle) myosin within the myosin mixture that was applied to the motility surface are shown with V_{actin} normalized to the faster cardiac myosin. The data are the combined results of two independent preparations for each mixture. The fits through the relationships were determined by using SigmaPlot 2001 based on the mixture model (19). For all relationships, the apparent curvature suggests that smooth-muscle myosin generates greater F_{avg} than any of the cardiac myosins, with the estimated relative F_{avg} (mean ± SE) for the smooth-muscle myosin (SM) to cardiac myosin as follows: SM/WT = 1.90 ± 0.13; SM/S532P = 2.35 ± 0.19; SM/F764L = 2.50 ± 0.14. Based on these fits and F_{avg} estimates, the resultant relationships between F_{avg} for the mutants relative to WT are presented in Table 3.

Materials and Methods

Generation of Mutant Mice. Knockin S532P and F764L cardiac MHC missense mutations were introduced into the murine α-cardiac MHC gene by using standard techniques (9, 34). Briefly, murine α-cardiac MHC gene sequences were isolated from a mouse 129/SvJ BAC library (Incyte Genomics, Palo Alto, CA). The targeting vector of the F764L mutation was constructed from two adjacent 2.1- and 4.3-kb-long EcoRI fragments spanning exons 16–19 and exons 20–24 and plasmid *pPNTloxPNeo* (Fig. 5). The missense mutation F764L, in exon 21, was introduced into an EcoRI-XhoI subfragment by using PCR mutagenesis before reinsertion into the plasmid. The S532P mutation, in exon 16, was introduced into the 2.1-kb EcoRI fragment, which encodes exons 16–19. The 2.1-kb EcoRI fragment carrying the S532P mutation and SpeI-EcoRI (3.7 kb; exons 9–15) flanked the PGK (phosphoglycerate kinase)-neomycin resistance gene (Fig. 5). For both constructs, the neomycin resistance cassette was placed in the middle of large introns. Plasmid constructs were linearized with NotI and used for transfection of ES cells (129/SvJ). G418-resistant clones were screened for homologous recombination by Southern blot analyses. Chimeric mice were mated with EIIa-Cre transgenic mice in the 129/SvEv background for deletion of the neomycin resistance gene. Genotypes were determined by PCR analysis and restriction digestion using mouse-tail DNA. The F764L mutation abolishes an MboII site, and the S532P mutation adds an MboI site. The expression of the mutation was confirmed by restriction digestion and by sequencing of standard RT-PCR products using primers that span several exons (Fig. 5). All mice used in these studies were bred onto the strain 129/SvEv background.

Mouse Echocardiography. Echocardiography of anesthetized mice (10 μl of 2.5% tribromoethanol per gram of body weight) was performed with a 6- to 15-MHz linear array probe connected to a Sonos 4500 ultrasonograph (Hewlett-Packard, Andover, MA) as described in refs. 35 and 36. Cardiac dimensions were obtained from M-mode tracings by using measurements averaged from three separate cardiac cycles. A single observer who did not know the mouse's genotype performed all echocardiographic studies. Cardiac contractile function was represented by the parameter LV fractional shortening (percentage), calculated as [(LV diastolic diameter − LV systolic diameter)/LV diastolic diameter] × 100.

Characterization of Single Cardiac Myocytes. Myocytes were isolated as described in ref. 37. An edge detection camera allowed simultaneous recordings of cell length changes in single myocytes. Myocytes in which contrast was insufficient to capture the outermost edge (cell length of <80 μm) were not included in analyses. Data were analyzed by using Digital Edge Detection Software from IonOptix (Milton, MA).

Ensemble and Single-Molecule Measurements. Myosin isolation, ATPase activities and actin filament velocities in the motility assay were measured as described in refs. 12, 13, and 19. In brief, samples of LVs (≈20 mg) were homogenized for 20 min in high-salt buffer (1:5 wt:vol, 0.3 M KCl/0.15 M K_2HPO_4/0.01 M Na_4PO_7/0.001 M $MgCl_2$/0.002 M DTT, pH 6.8), followed by ultracentrifugation for 1 h at 150,000 × *g*. Filamentous myosin was precipitated from the supernatant, pelleted by ultracentrifugation for 20 min at 50,000 × *g*, and resuspended in myosin buffer (0.025 M imidazole/0.004 M $MgCl_2$/0.01 M DTT/0.001 M EGTA/0.3 M KCl, pH 7.4). This mini-isolation procedure, used extensively in our laboratory (15, 29, 38), yields ≈0.2 mg of highly purified whole myosin without evidence of protein contaminants or proteolysis. Additionally, before an experiment, the myosin was further purified by centrifugation in the presence of equimolar actin and 0.001 M ATP in myosin buffer (15). By using only the supernatant, denatured "rigor-like" myosin that would have dramatic impeding effects in the motility assay and laser trap was eliminated.

The detailed procedures for the actomyosin ATPase measurements are described in refs. 29 and 38. In brief, actin-activated ATPase activities of myosin (100–400 nM) isolated from a single heart were measured through colorimetric determination of P_i release at multiple actin concentrations between 5 and 20 μmol/liter by using 2 mmol/liter MgATP at pH 7.4 and 20°C. Values of P_i released (s^{-1}·$head^{-1}$) versus actin concentration were plotted and fitted to Michaelis–Menten kinetics ($V = V_{max} \times [actin]/K_m + [actin]$) with V_{max} and K_m fit parameters by using SigmaPlot 2001.

Actin filament velocities (V_{actin}) were determined in an *in vitro* motility assay (12, 15) through manual filament tracking software (13) at 1 mM ATP in low-salt actin buffer (0.025 M imidazole/0.004 M $MgCl_2$/0.01 M DTT/0.001 M EGTA/0.025 M KCl, pH 7.4) at 30°C, and 100 μg/ml monomeric myosin was added to the flow-cell chamber. Video images were digitized at three frames per s so that actin filaments moved no more than half their length between images. Up to 50 filaments per heart sample were tracked within a field in which >90% of the filaments were moving. For each filament, its mean velocity and SD were determined, and filaments having a SD of the mean velocity of 30% or better were accepted, which was indicative of a continuous and smoothly moving actin filament (39). The velocity data in Table 3 are reported for multiple hearts as the mean and SD based on the mean velocity of the recorded filaments for each heart.

To measure the relative maximum average isometric force

(F_{avg}), a myosin mixtures assay was used (19). In this assay, fast (cardiac) and slow (chicken gizzard smooth muscle) myosins were mixed in various proportions to a total concentration of 100 μg/ml and then added to the experimental chamber under the conditions described above. The relationship of V_{actin} versus the myosin mixture ratio was fitted to a model that assumes that the force-generating capacity for the two myosins within the mixture are affecting each other's motion generation because of their simultaneous interaction with a given actin filament (see ref. 19 for model details). The model fit, using SigmaPlot 2001 software, provides an estimate of the relative F_{avg} for the fast and slower myosin. This indirect assay has been validated through direct measures of force generation, albeit by using an extremely labor-intensive microneedle assay (21, 40).

The laser trap techniques are described in detail in ref. 18. Briefly, two orthogonally polarized beams were split from a single beam generated by a variable power Nd:yttrium/aluminum-garnet solid-state laser (transverse electromagnetic mode 00, maximum power 2.5 W, 1,064 nm; model T-10V-106C; Spectra Physics, Mountain View, CA). Each beam trapped a *N*-ethylmaleimide-myosin-coated polystyrene bead that was attached to the ends of a fluorescently labeled actin filament, with a typical single trap stiffness of ≈0.02 pN/nm and 4 pN of pretension. The bead–actin–bead system was brought into close proximity of the surface of a silica bead pedestal that was sparsely coated with myosin. Unitary displacement events were detected as changes in the bright-field image position of one of the trapped beads. This image was projected onto a quadrant photodiode detector with bead displacement indicating unitary displacements. Data traces (Fig. 3) were analyzed by using the mean-variance technique as described in ref. 18 to obtain estimates of unitary step size and the duration of strong actin binding. All experiments were performed at 25°C and in low-salt actin buffer with 10 μM ATP.

Statistical Analysis. Statistical analysis was performed by using SigmaStat 3.0 (SPSS, Point Richard, CA). A one-way ANOVA was used to determine significance, and a Student–Neuman–Keuls post hoc test was used to locate specific differences among the means. $P < 0.05$ was considered significant.

We thank X. Xu for preparation of myocytes, M. Babl for preparation of histological sections, and Guy Kennedy for support of the mechano-optical instrumentation. This work was supported by the Henrietta and Frederick Bugher Fund (J.G.S.), the Howard Hughes Medical Institute (C.E.S.), the National Institutes of Health (D.W., C.E.S., and J.G.S.), and the Deutsche Stiftung für Herzforschung (J.P.S.).

1. Thom T, Haase N, Rosamond W, Howard VJ, Rumsfeld J, Manolio T, Zheng ZJ, Flegal K, O'Donnell C, Kittner S, *et al.* (2006) *Circulation* 113:e85–e151.
2. Colluci WS, Braunwald EB (1997) in *Heart Disease*, ed Braunwald E (Saunders, Philadelphia), pp 394–420.
3. Towbin JA, Bowles NE (2002) *Expert Rev Mol Diagn* 2:587–602.
4. Seidman JG, Seidman C (2001) *Cell* 104:557–567.
5. Daehmlow S, Erdmann J, Knueppel T, Gille C, Froemmel C, Hummel M, Hetzer R, Regitz-Zagrosek V (2002) *Biochem Biophys Res Commun* 298:116–120.
6. Kamisago M, Sharma SD, DePalma SR, Solomon S, Sharma P, McDonough B, Smoot L, Mullen MP, Woolf PK, Wigle ED, *et al.* (2000) *N Engl J Med* 343:1688–1696.
7. Warshaw DM (1996) *News Physiol Sci* 11:1–7.
8. Rayment I, Holden HM, Sellers JR, Fananapazir L, Epstein ND (1995) *Proc Natl Acad Sci USA* 92:3864–3868.
9. Geisterfer-Lowrance AA, Christe M, Conner DA, Ingwall JS, Schoen FJ, Seidman CE, Seidman JG (1996) *Science* 272:731–734.
10. Wang Q, Moncman CL, Winkelmann DA (2003) *J Cell Sci* 116:4227–4238.
11. Schmitt JP, Kamisago M, Asahi M, Li GH, Ahmad F, Mende U, Kranias EG, MacLennan DH, Seidman JG, Seidman CE (2003) *Science* 299:1410–1413.
12. Warshaw DM, Desrosiers JM, Work SS, Trybus KM (1990) *J Cell Biol* 111:453–463.
13. Work SS, Warshaw DM (1992) *Anal Biochem* 202:275–285.
14. Baker JE, Brosseau C, Joel PB, Warshaw DM (2002) *Biophys J* 82:2134–2147.
15. Palmiter KA, Tyska MJ, Haeberle JR, Alpert NR, Fananapazir L, Warshaw DM (2000) *J Muscle Res Cell Motil* 21:609–620.
16. Rayment I, Holden HM, Whittaker M, Yohn CB, Lorenz M, Holmes KC, Milligan RA (1993) *Science* 261:58–65.
17. Volkmann N, Ouyang G, Trybus KM, DeRosier DJ, Lowey S, Hanein D (2003) *Proc Natl Acad Sci USA* 100:3227–3232.
18. Guilford WH, Dupuis DE, Kennedy G, Wu J, Patlak JB, Warshaw DM (1997) *Biophys J* 72:1006–1021.
19. Harris DE, Work SS, Wright RK, Alpert NR, Warshaw DM (1994) *J Muscle Res Cell Motil* 15:11–19.
20. Alpert NR, Brosseau C, Federico A, Krenz M, Robbins J, Warshaw DM (2002) *Am J Physiol* 283:H1446–H1454.
21. VanBuren P, Harris DE, Alpert NR, Warshaw DM (1995) *Circ Res* 77:439–444.
22. Woledge RC, Curtin NA, Homsher E (1985) *Monogr Physiol Soc* 41:1–357.
23. Debold EP, Patlak JB, Warshaw DM (2005) *Biophys J* 89:L34–L36.
24. Ahmad F, Seidman JG, Seidman CE (2005) *Annu Rev Genomics Hum Genet* 6:185–216.
25. Georgakopoulos D, Christe ME, Giewat M, Seidman CM, Seidman JG, Kass DA (1999) *Nat Med* 5:327–330.
26. Maron BJ (2002) *J Am Med Assoc* 287:1308–1320.
27. Keller DI, Coirault C, Rau T, Cheav T, Weyand M, Amann K, Lecarpentier Y, Richard P, Eschenhagen T, Carrier L (2004) *J Mol Cell Cardiol* 36:355–362.
28. Yamashita H, Tyska MJ, Warshaw DM, Lowey S, Trybus KM (2000) *J Biol Chem* 275:28045–28052.
29. Tyska MJ, Hayes E, Giewat M, Seidman CE, Seidman JG, Warshaw DM (2000) *Circ Res* 86:737–744.
30. Fatkin D, Graham RM (2002) *Physiol Rev* 82:945–980.
31. Ingwall JS (2004) *J Mol Cell Cardiol* 37:613–623.
32. Olson EN (2004) *Nat Med* 10:467–474.
33. Mirza M, Marston S, Willott R, Ashley C, Mogensen J, McKenna W, Robinson P, Redwood C, Watkins H (2005) *J Biol Chem* 280:28498–28506.
34. Bruneau BG, Nemer G, Schmitt JP, Charron F, Robitaille L, Caron S, Conner DA, Gessler M, Nemer M, Seidman CE, Seidman JG (2001) *Cell* 106:709–721.
35. Fatkin D, Christe ME, Aristizabal O, McConnell BK, Srinivasan S, Schoen FJ, Seidman CE, Turnbull DH, Seidman JG (1999) *J Clin Invest* 103:147–153.
36. Fatkin D, McConnell BK, Mudd JO, Semsarian C, Moskowitz IG, Schoen FJ, Giewat M, Seidman CE, Seidman JG (2000) *J Clin Invest* 106:1351–1359.
37. Semsarian C, Ahmad I, Giewat M, Georgakopoulos D, Schmitt JP, McConnell BK, Reiken S, Mende U, Marks AR, Kass DA, *et al.* (2002) *J Clin Invest* 109:1013–1020.
38. Nguyen TT, Hayes E, Mulieri LA, Leavitt BJ, ter Keurs HE, Alpert NR, Warshaw DM (1996) *Circ Res* 79:222–226.
39. Homsher E, Kim B, Bobkova A, Tobacman LS (1996) *Biophys J* 70:1881–1892.
40. VanBuren P, Waller GS, Harris DE, Trybus KM, Warshaw DM, Lowey S (1994) *Proc Natl Acad Sci USA* 91:12403–12407.